PHILOSOPHICAL TRANSACTIONS OF THE ROYAL SOCIETY A

Phil. Trans. R. Soc. A (2011) **369**, 3447–3455
doi:10.1098/rsta.2011.0122

Characterization of the tunable response of highly strained compliant optical metamaterials

By Imogen M. Pryce[1,†], Koray Aydin[1,†], Yousif A. Kelaita[1], Ryan M. Briggs[1] and Harry A. Atwater[1,2,*]

[1]*Thomas J. Watson Laboratories of Applied Physics, and*
[2]*Kavli Nanoscience Institute, California Institute of Technology, 1200 East California Boulevard, Pasadena, CA 91125, USA*

Metamaterial designs are typically limited to a narrow operating bandwidth that is predetermined by the fabricated dimensions. Various approaches have previously been used to introduce post-fabrication tunability and thus enable active metamaterials. In this work, we exploit the mechanical deformability of a highly compliant polymeric substrate to achieve dynamic, tunable resonant frequency shifts greater than a resonant linewidth. We investigate the effect of metamaterial shape on the plastic deformation limit of resonators. We find that, for designs in which the local strain is evenly distributed, the response is elastic under larger global tensile strains. The plastic and elastic limits of resonator deformation are explored and the results indicate that, once deformed, the resonators operate within a new envelope of elastic response. We also demonstrate the use of coupled resonator systems to add an additional degree of freedom to the frequency tunability and show that compliant substrates can be used as a tool to test coupling strength. Finally, we illustrate how compliant metamaterials could be used as infrared sensors, and show enhancement of an infrared vibration absorption feature by a factor of 225.

Keywords: metamaterial; mechanical deformation; infrared sensors

1. Introduction

Electromagnetic metamaterials are composites engineered at the subwavelength scale to have specific optical properties. Behaviour that is unattainable in any of the constituent materials can be demonstrated by carefully designing individual unit cells [1,2]. In most cases, this behaviour is fixed at the time of fabrication and yields materials with a passive response over a limited bandwidth. Active metamaterials control the resonant response of a material by incorporating dynamic components at the unit cell or substrate level and represent a new class of resonant structures. Introducing tunability by controllably activating a metamaterial system is important for the development of a number of devices including modulators, tunable filters and concentrators. Several approaches, ranging from electrical probing of single unit cells to thermal actuation, have

*Author for correspondence (haa@caltech.edu).
†These authors contributed equally to the study.

One contribution of 9 to a Theo Murphy Meeting Issue ‘Metallic metamaterials and plasmonics’.

been used to demonstrate amplitude modulation and frequency tuning of the resonant response [3–8]. In this work, we explore how a polymer substrate can be used as the dynamic component of an active metamaterial, enabling mechanical deformation of the composite unit cells.

Flexible, stretchable platforms for electronics are an increasingly popular concept because of the ease with which they could be integrated with other devices [9]. In the realm of plasmonic structure design, elastomeric substrates have been used to alter the resonant response of nanoparticle dimers and gratings [10,11]. In a previous paper, we showed that mechanical actuation of a surface can be used to achieve a linewidth shift in the resonant response of a metamaterial surface [12]. Although other reports have demonstrated the utility of flexible metamaterials operating at microwave [13] and terahertz [14,15] frequencies, this was the first report of greater-than-linewidth tuning in the near infrared. In this paper, we explore how compliant substrates can be used to tune the resonant frequencies of various split ring resonator (SRR) designs and show that coupling two resonators enables broader tunability. We also investigate the dependence of the mechanical deformation on resonator shape and the limits of plastic and elastic tunability of polymer-embedded resonator systems.

2. Fabrication and measurement techniques

The metamaterial surfaces investigated are arrays of Au SRRs in which the geometry and the refractive indices of the metal and the host substrate affect the resonant frequency. These types of resonator geometries have been studied extensively in the optical regime [16,17]. They can be modelled as LC circuits with a resonant frequency, $\omega_0 \sim (LC)^{-1/2}$, where the distributed inductance (L) is dependent on the total path length of the resonator, and the distributed capacitance (C) is inversely proportional to the distance between the SRR arms.

We use a hard/soft nanolithographic pattern transfer technique to investigate a number of different SRR designs. SRR arrays are patterned in polymer resist over $100 \times 100\,\mu\text{m}$ squares by electron beam lithography on a sacrificial Si substrate. Au is evaporated using electron beam evaporation to create 100 nm thick patterns (figure 1*a*; step 1). The Au is functionalized with a monolayer of 3-mercaptopropyl trimethoxysilane (MPT) under a 50 mTorr vacuum. This serves to improve adhesion between the Au resonators and a polydimethylsiloxane (PDMS) layer that is cured on top of the patterns (figure 1*b*; step 2). The Si handle substrate is selectively removed via low-bias inductively coupled plasma-reactive ion etching (ICP-RIE) with SF_6, leaving free-standing PDMS substrates patterned with multiple arrays of Au SRRs (figure 1*c*; step 3). The schematics in figure 1 outline this process and show how a typical pattern, an SRR with a bar resonator, is transferred to the PDMS. Figure 1*a* shows an electron micrograph of the pattern on the Si wafer after electron beam patterning. The micrograph in figure 1*c* shows the pattern on the PDMS after transfer, demonstrating that the nanostructures do not undergo any kind of deterioration in the transfer process. The transfer process is reproducible for a number of designs with nanometre feature sizes and has been replicated for many different samples.

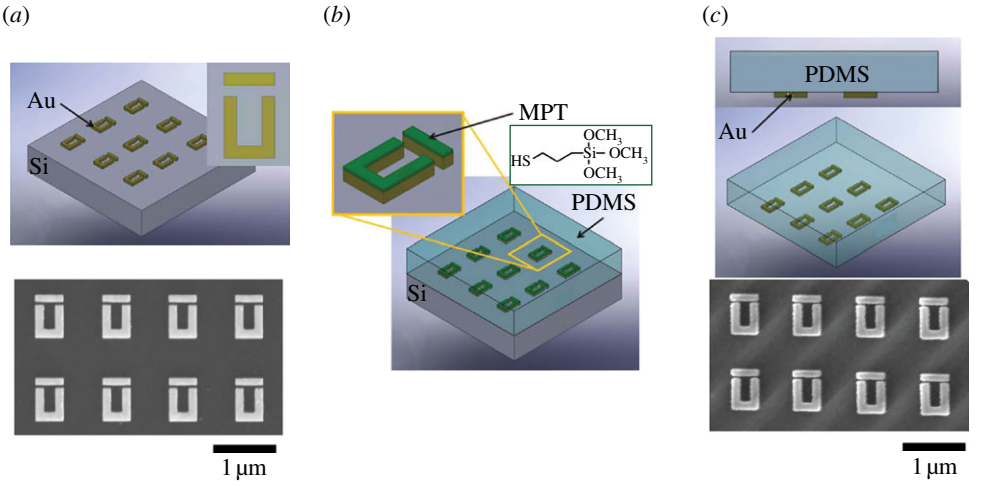

Figure 1. The schematic shows the sequence for fabricating compliant metamaterials. (*a*) The first step illustrates how the SRRs are lithographically patterned on a Si handle wafer. The SRR–nanowire-coupled resonator pair is used as an example, but the same approach is followed for all resonator types. The scanning electron micrograph shows the resonators as patterned on Si. (*b*) The second step shows how the Au is functionalized with MPT and embedded in PDMS. (*c*) Last, the Si wafer is back-etched via RIE to leave a free-standing PDMS substrate. The SEM in this panel shows the fidelity of the pattern transfer. (Online version in colour.)

A custom-built stage is used to mechanically deform the samples, change the resonator shape and shift the resonant frequency. The strain is defined as $(l - l_0)/l_0 \times 100\%$, where l_0 is the initial length of the sample and l is the stretched length. We characterize the samples via environmental scanning electron microscopy (SEM) to determine the mechanical deformation to the individual resonators. We also use a Fourier transform infrared (FTIR) spectrometer in reflection mode to characterize the effect of strain on the resonance of the SRRs. The reflectance is normalized to an Au reflection standard.

3. Basic split ring resonator designs

We first investigate basic SRR designs and compare a circular SRR (CSRR) design (figure 2*a*) with a square SRR (SSRR) design (figure 2*b*). The initial resonance at 5.04 µm (dashed line) is for the pattern after transfer from the Si to the PDMS and prior to stretching. Straining the resonators in the direction parallel to the gap causes the gap to decrease and the capacitance to increase. As is evident from the expression for ω_0, increasing the capacitance will decrease the resonant frequency and red-shift the resonant wavelength. For a strain of 10 per cent, the resonance shifts by 60 nm to 5.10 µm. The resonators were strained up to 50 per cent, which red-shifts the resonance by 140 nm to 5.18 µm. The total path length of the SSRR is shorter than that of the CSRR and, consequently, the initial resonance is at a shorter wavelength. This is indicated by the leftmost dashed line and occurs at 4.56 µm (figure 2*b*). For the SSRR,

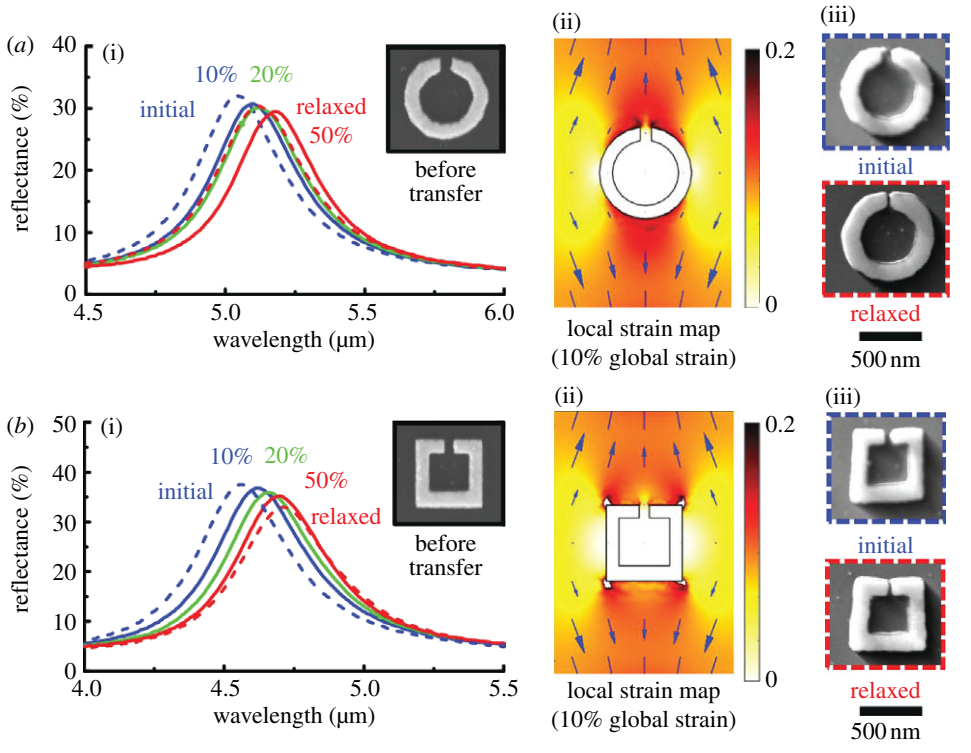

Figure 2. (*a*) (i) The FTIR spectra for a circular SRR (CSRR) for strains of up to 50%. The inset of this graph shows the resonator on Si prior to transfer to the PDMS. (ii) The local strain map for a CSRR as calculated using FEM modelling. The colour map corresponds to the local strain induced in the resonator, while the arrows indicate the local displacement. (iii) Environmental SEM images of a single resonator after transfer ('initial') and after mechanical deformation ('relaxed'). The same data for the square SRR (SSRR) are shown in (*b*). (Online version in colour.)

we find that stretching the structure to a global strain of 10 per cent induces a shift of 60 nm to 4.62 μm, while a strain of 50 per cent shifts the resonance by 140 nm to 4.70 μm.

Although the induced shifts in resonance are the same for both of these structures, there is a noticeable difference between the CSRR and the SSRR structures. When the samples are allowed to relax after stretching to 50 per cent strain, the resonance of the CSRR (figure 2*a*) moves to a value between the initial resonance and the fully strained resonance, whereas the SSRR resonance remains at the fully strained resonance. In order to better understand the mechanical deformation, the structures were modelled using finite-element method (FEM) continuum mechanics calculations. The results of these calculations are shown in the strain maps in figure 2*a*,*b*. The colour intensity of the image indicates the local strain induced for 10 per cent global strain, while the arrows show the displacement. It is evident that, for the CSRR, the strain is distributed around the outside of the Au, with small regions of high strain concentrated at the gap. The strain on the SSRR, however, is highly localized at the corners of the resonator. This high strain density causes

irreversible deformation of the Au–PDMS system upon stretching. These results are corroborated by the environmental SEM images shown in figure 2. In the case of the CSRR design, the SEM micrograph shows that the pattern changes much less dramatically upon transfer to the PDMS. When the sample is relaxed, the gap size decreases, but the shape of the ring is not distorted. For the square ring, the shape is already slightly distorted after transfer to the PDMS and, after relaxing, the arms are obviously bowed inwards. Both of these structures are useful for guiding future resonator designs. For designs where an elastic response is important, we would want to ensure that there are no regions of high strain density upon stretching. For designing resonators where deformation is used to permanently tune the resonance to a specific value, high regions of local strain could be exploited to give predetermined resonator shapes.

4. Coupled resonator systems

The basic split ring designs allow control over the capacitance but lead to limited tuning of the resonance. In order to achieve linewidth-scale tunability of the resonant frequency, we introduce another resonator to the system in such a way that the resonators are coupled. By changing the distance between the coupled resonators, we can affect the coupling constant, changing the resonant frequency. In previous work, we used passive structures to show that a change in the coupling constant shifts the resonant frequency [16]. We also used asymmetric coupled SRRs to show how the resonant hybridization effect of the two resonators can be exploited to demonstrate linewidth tunability on a compliant substrate [12].

In figure 3, we introduce a nanowire resonator coupled to a basic 'U'-shaped resonator. The top line shows the resonant frequency for a nanowire–SRR system where the distance between resonators, d, is 110 nm. We patterned three other arrays of nanowire–SRRs with distances of 90 nm, 70 nm and 50 nm. The electron micrographs of each of these designs on Si prior to transfer are shown to the right of the FTIR spectra. The dashed lines indicate the shift of the resonant peak with 5 per cent strain. In the case of the $d = 110$ nm system, 5 per cent strain causes no shift in the resonant peak position. As the initial coupling distance decreases, however, the introduction of 5 per cent strain does cause a shift in resonance. For the $d = 90$ nm case, the resonance shifts 10 nm, and, for the $d = 70$ nm resonator pair, the peak shift is 50 nm. Finally, for the $d = 50$ nm system, the peak shifts by 80 nm from 3.65 to 3.57 μm, a significant fraction of the linewidth. This illustrates that, for systems where the resonators are closer together and thus more strongly coupled, small changes in the coupling distance will have a more pronounced effect on resonant peak position.

Compliant metamaterial surfaces could potentially be used as infrared sensors, or surface-enhanced infrared absorption substrates [18–20]. In figure 3*a*, there is a noticeable reflection dip at 3.37 μm for the $d = 90$ nm and $d = 100$ nm cases. This absorption feature corresponds to the vibrational mode of a C–H stretch bond of PDMS [21]. In figure 3*b*, we plot the intensity of the reflection dip for each resonator divided by the reflection dip of the peak for bare PDMS. First,

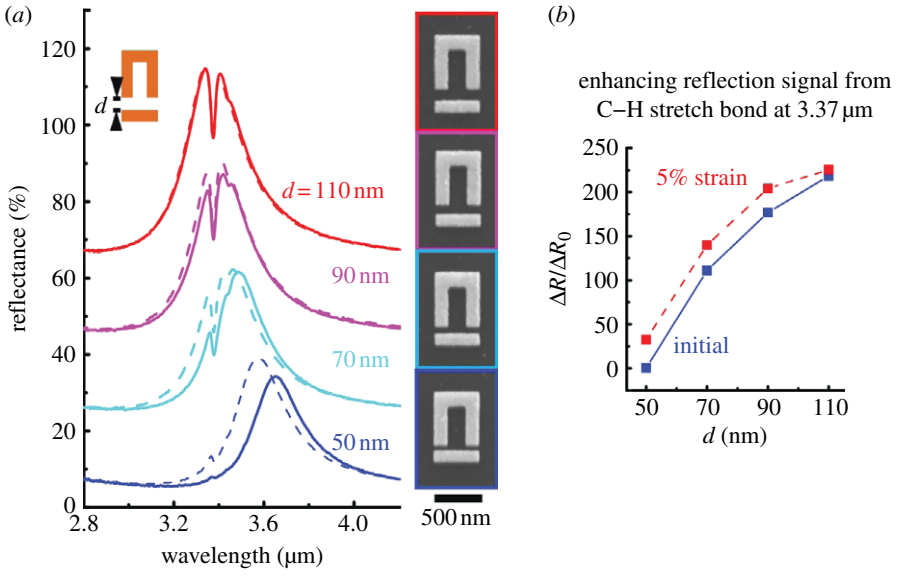

Figure 3. (*a*) The FTIR spectra for various SRR–nanowire-coupled resonator pair arrays are shown. The spacing d is varied from $d = 110$ nm to $d = 50$ nm. Each dashed line shows how 5% global strain affects the resonant peak position. The SEM images to the right of the FTIR data show the SRR-bar designs on Si prior to transferring to PDMS. (*b*) The change in reflection for the absorption feature corresponding to the vibrational mode of the C–H stretch bond in PDMS is shown. The change is reported relative to the reflection dip for bare PDMS. The data for both the initial position (solid line) and the 5% strain (dashed line) resonant peak position are reported. (Online version in colour.)

we see that, as each resonator is strained and the enhancement moves from the solid to the dashed line, the enhancement of the absorption feature increases. This is a result of shifting the resonance of the SRR closer to the resonance of the vibrational mode. Additionally, the resonance of the $d = 110$ nm SRR matches the vibrational mode most closely and hence results in over a 200-fold enhancement of the reflection dip before stretching. When this array of resonators is stretched, the enhancement of the absorption feature increases to 225. In previous work, we showed that large strains could be applied to match the resonant frequency and increase the signal strength. In this case, we show how a small amount of strain (5%) can be used to optimize the resonance of a resonator designed to operate at a particular frequency.

5. Larger strain and changes in elasticity

Full linewidth tunability is an important goal for any active metamaterial as it is critical for a number of applications, including optical filters and modulators. In figure 4*a*, we demonstrate the effects of larger strain on the $d = 50$ nm SRR-bar coupled resonator system. For a strain of 20 per cent, the resonant peak blue-shifts to 3.56 μm from the initial resonance position of 3.64 μm. Instead of

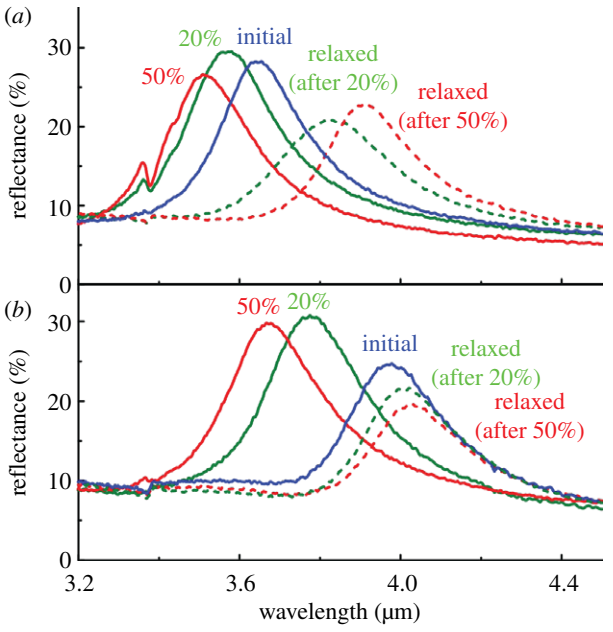

Figure 4. (*a*) Initial plastic deformation: FTIR spectra for the $d = 50$ nm SRR–nanowire-coupled resonator pair under tensile strains of up to 50% are shown. (*b*) Subsequent loading behaviour: FTIR spectra for tensile strains of up to 50% are shown. The corresponding 0% strain position ('relaxed (after 20%)' and 'relaxed (after 50%)') data are shown to demonstrate the elastic nature of the resonator after initial deformation. (Online version in colour.)

relaxing back to the initial resonance, the peak relaxes to a frequency that is further red-shifted owing to permanent deformation of the PDMS in the gap. Similar behaviour occurs for a strain of 50 per cent where the resonant peak shifts to a wavelength of 3.51 μm and then relaxes back to a resonant frequency that is even further red-shifted at 3.91 μm. Though the 50 per cent strain resonant peak position is not a full linewidth shift from the initial position, it is a linewidth shift from its relaxed position.

Elasticity of the response is an important criterion for active metamaterials, and we show here, as in previous work, that for strains of more than 10 per cent the samples have an inelastic response. In figure 4*b*, however, we examine the sample response after deformation to a tensile strain of 50 per cent. In this case, the initial position is the same as the 'relaxed (after 50%)' position in figure 4*a*. The resonant peak position shifts to 3.77 μm for a strain of 20 per cent. Of particular interest here is that the sample relaxes back to the initial resonance. Similar behaviour is observed when the sample is stretched to 50 per cent strain and the peak blue-shifts by 330 nm to 3.67 μm, a full linewidth from the initial resonance. These data show that, once deformation has been introduced to a sample, there is a new elastic deformation limit. This means that subsequent loading cycles, like that shown in figure 4*b*, give information about sample strain history. In addition, it shows that we can initially introduce deformation to achieve an elastically tunable response.

6. Conclusions

Using mechanical deformation of a compliant substrate to achieve an active response in metamaterial surfaces sets the stage for new types of metamaterial design. Metamaterials were previously restricted to hard, brittle substrates, but attaching patterns to an elastomeric substrate enables their use in flexible electronics and allows post-fabrication adjustments of their properties. In this work, we have explored how different shapes can affect the local mechanical properties of a device. For designs that experience high local strain, we found that the deformation for low global strain is plastic and fixes the final resonance position. When the local strain is evenly distributed across a structure, the deformation is much more likely to be elastic in nature. Coupled resonator pairs were used to illustrate how the coupling constant affects the resonant frequency of a particular SRR design. Strongly coupled resonator pairs lead to improved tunability of the design, which is of particular importance in the design of metamaterial-based optical filters and modulators. We also investigated how these resonators could be used as metamaterial-based sensors and show that the absorption feature corresponding to the vibrational mode of the C–H stretch bond can be enhanced 225 times. An important feature of any active metamaterial is the elasticity of its response and in this work we have explored how mechanical deformation can set new limits for elastic tunability.

Financial support from the Air Force Office of Scientific Research under grant no. FA9550-09-1-0673 is appreciated. I.M.P. acknowledges the support of a National Science Foundation Fellowship. We gratefully acknowledge critical support and infrastructure provided for this work by the Kavli Nanoscience Institute at Caltech. Portions of this work were performed in facilities sponsored by the Center for Science and Engineering of Materials, an NSF MRSEC. We gratefully acknowledge Professor George Rossman for access to his IR facilities and invaluable discussions. We thank Dr Shannon Boettcher and Elizabeth Santori for help with surface functionalization and David Valley and Vivian Ferry for useful discussions.

References

1 Shalaev, V. M. 2007 Optical negative-index metamaterials. *Nat. Photon.* **1**, 41–48. (doi:10.1038/nphoton.2006.49)

2 Smith, D. R., Pendry, J. B. & Wiltshire, M. C. K. 2004 Metamaterials and negative refractive index. *Science* **305**, 788–792. (doi:10.1126/science.1096796)

3 Chen, H.-T., Padilla, W. J., Zide, J. M. O., Gossard, A. C., Taylor, A. J. & Averitt, R. D. 2006 Active terahertz metamaterial devices. *Nature* **444**, 597–600. (doi:10.1038/nature05343)

4 Tao, H., Strikwerda, A. C., Fan, K., Padilla, W. J., Zhang, X. & Averitt, R. D. 2009 Reconfigurable terahertz metamaterials. *Phys. Rev. Lett.* **103**, 147401. (doi:10.1103/PhysRevLett.103.147401)

5 Dicken, M. J., Aydin, K., Pryce, I. M., Sweatlock, L. A., Boyd, E. M., Walavalkar, S., Ma, J. & Atwater, H. A. 2009 Frequency tunable near-infrared metamaterials based on VO_2 phase transition. *Opt. Express* **17**, 18 330–18 339. (doi:10.1364/OE.17.018330)

6 Sámson, Z. L., MacDonald, K. F., De Angelis, F., Gholipour, B., Knight, K., Huang, C. C., Di Fabrizio, E., Hewak, D. W. & Zheludev, N. I. 2010 Metamaterial electro-optic switch of nanoscale thickness. *Appl. Phys. Lett.* **96**, 143105. (doi:10.1063/1.3355544)

7 Xiao, S. M., Chettiar, U. K., Kildishev, A. V., Drachev, V., Khoo, I. C. & Shalaev, V. M. 2009 Tunable magnetic response of metamaterials. *Appl. Phys. Lett.* **95**, 033115. (doi:10.1063/1.3182857)

8 Chen, H. T., O'Hara, J. F., Azad, A. K., Taylor, A. J., Averitt, R. D., Shrekenhamer, D. B. & Padilla, W. J. 2008 Experimental demonstration of frequency-agile terahertz metamaterials. *Nat. Photon.* **2**, 295–298. (doi:10.1038/nphoton.2008.52)

9 Rogers, J. A., Someya, T. & Huang, Y. G. 2010 Materials and mechanics for stretchable electronics. *Science* **327**, 1603–1607. (doi:10.1126/science.1182383)

10 Cole, R. M., Mahajan, S. & Baumberg, J. J. 2009 Stretchable metal-elastomer nanovoids for tunable plasmons. *Appl. Phys. Lett.* **95**, 154103. (doi:10.1063/1.3247966)

11 Olcum, S., Kocabas, A., Ertas, G., Atalar, A. & Aydinli, A. 2009 Tunable surface plasmon resonance on an elastomeric substrate. *Opt. Express* **17**, 8542–8547. (doi:10.1364/OE.17.008542)

12 Pryce, I. M., Aydin, K., Kelaita, Y. A., Briggs, R. M. & Atwater, H. A. 2010 Highly strained compliant optical metamaterials with large frequency tunability. *Nano Lett.* **10**, 4222–4227. (doi:10.1021/Nl102684x)

13 Melik, R., Unal, E., Perkgoz, N. K., Puttlitz, C. & Demir, H. V. 2009 Flexible metamaterials for wireless strain sensing. *Appl. Phys. Lett.* **95**, 181105. (doi:10.1063/1.3250175)

14 Tao, H. *et al.* 2008 Highly flexible wide angle of incidence terahertz metamaterial absorber: design, fabrication, and characterization. *Phys. Rev. B* **78**, 241103(R). (doi:10.1103/Physrevb.78.241103)

15 Tao, H., Strikwerda, A. C., Fan, K., Bingham, C. M., Padilla, W. J., Zhang, X. & Averitt, R. D. 2008 Terahertz metamaterials on free-standing highly-flexible polyimide substrates. *J. Phys. D Appl. Phys.* **41**, 232004. (doi:10.1088/0022-3727/41/23/232004)

16 Aydin, K., Pryce, I. M. & Atwater, H. A. 2010 Symmetry breaking and strong coupling in planar optical metamaterials. *Opt. Express* **18**, 13 407–13 417. (doi:10.1364/OE.18.013407)

17 Sersic, I., Frimmer, M., Verhagen, E. & Koenderink, A. F. 2009 Electric and magnetic dipole coupling in near-infrared split-ring metamaterial arrays. *Phys. Rev. Lett.* **103**, 213902. (doi:10.1103/PhysRevLett.103.213902)

18 Lal, S., Grady, N. K., Kundu, J., Levin, C. S., Lassiter, J. B. & Halas, N. J. 2008 Tailoring plasmonic substrates for surface enhanced spectroscopies. *Chem. Soc. Rev.* **37**, 898–911. (doi:10.1002/chin.200832239)

19 Neubrech, F., Pucci, A., Cornelius, T. W., Karim, S., Garcia-Etxarri, A. & Aizpurua, J. 2008 Resonant plasmonic and vibrational coupling in a tailored nanoantenna for infrared detection. *Phys. Rev. Lett.* **101**, 157403. (doi:10.1103/PhysRevLett.101.157403)

20 Cubukcu, E., Zhang, S., Park, Y. S., Bartal, G. & Zhang, X. 2009 Split ring resonator sensors for infrared detection of single molecular monolayers. *Appl. Phys. Lett.* **95**, 043113. (doi:10.1063/1.3194154)

21 Smith, A. L. & Anderson, D. R. 1984 Vibrational spectra of Me_2SiCl_2, Me_3SiCl, $Me_3SiOSiMe_3$, $(Me_2SiO)_3$, $(Me_2SiO)_4$, $(Me_2SiO)_x$, and their deuterated analogs. *Appl. Spectrosc.* **38**, 822–834. (doi:10.1366/0003702844554549)